# Ruthenium ion modification of glassy carbon: implication on the structural evolution and migration behaviour of implanted Ru atoms

T.A.O. Jafer[1], T.T. Thabethe[1], O.S. Odutemowo[1], S.A. Adeojo[1,2], H.A.A. Abdelbagi[1,3], A. Azarov[4], J.B. Malherbe[1]

*[1]Physics Department, University of Pretoria, Pretoria, South Africa*
*[2]Department of Physics and Engineering Physics, Obafemi Awolowo University, Ile-Ife*
*[3]Physics Department, Shendi University, Shendi, Sudan*
*[4]Department of Physics, Centre for Materials Science and Nanotechnology, University of Oslo, N-0316, Oslo, Norway*

## Abstract

Glassy carbon samples were implanted with ruthenium ions to a fluence of $1\times10^{16}$ $cm^{-2}$ at room temperature (at 150 keV). The implanted samples were annealed isochronally in vacuum from 1000 to 1300 °C for 5 hours. The resulting microstructural changes were investigated using X-ray diffraction (XRD), Raman spectroscopy andatomic force microscopy (AFM). The diffusion behaviour of ruthenium in glassy carbon was investigated using secondary-ion mass spectrometry (SIMS). Raman results showed that the implantation of ruthenium into glassy carbon caused amorphization and increase the tensile stress in the implanted region. XRD showed that the amount of tensile stress in virgin glassy carbon increased from 0.016 GPa to 0.19 GPa after ion implantation which is in qualitative agreement with the Raman results. Annealing of the samples exhibited more recrystallization and changed the tensile stress to compressive stress. SIMS results showed that annealing of the as-implanted samples at 1000 °C caused aggregation of the ruthenium atoms, while annealing at higher temperatures led to some segregation of ruthenium atoms at a depth of 155 nm below the glassy carbon surface. The aggregation of ruthenium atoms after annealing (as observed by SIMS) played a role in the surface roughness as observed by AFM.

**Keywords**: Implantation, Aggregation, Migration, Ruthenium, Glassy Carbon.

## 1. Introduction

Generating sustainable energy with minimized carbon footprint is a global challenge. Conventional fossil fuel method of generating energy is accompanied with the production of a huge amount of carbon dioxide, which inturn contributes to the climate change. In terms of its carbon footprint, nuclear energy is one of the cleanest sources, with almost negligible carbon emissions [1]. The nuclear power source is the most predictable and documented of all radioactive waste sources. Harnessing nuclear power comes with the production of enormous nuclear waste and there is a need for proper management of such waste. For example, a nuclear reactor operating with 1GW generates almost 20,000 – 27,000 kg of spent nuclear fuel (SNF) per year [2]. Thisradioactive waste becomes hazardous to human health when it escapes into the environmentduring waste transportation, storage, or accidental conditions [3]. Thus, it is crucial to manage the waste and its storage properly. Nuclear waste management has been a problem and concern for the nuclear industry; thus, a lot of countries have shied away from the use of nuclear [4].

The development of highly durable nuclear waste containers is a major consideration in nuclear waste management. Nuclear waste containers must ensure the long-term stability of radioactive materials, isolation of radioactivity during transportation, interim storage and disposal, and non-leakage from the container. Most nuclear waste containers are usually made of metals such as stainless steel, iron, copper, nickel-based alloys and titanium alloys [5]. These materials are susceptible to degradation due to ageing which can lead to leakage of radioactive material into the environment. Therefore, nuclear storage containers with a longer life span are necessary for nuclear waste. This can be achieved by improving the material from which the casks (i.e., nuclear storage containers) are made. Glassy carbon has been considered a storage container to immobilize nuclear waste against the traditional glass matrixes [6]. It is a form of synthetic carbon that exhibits glassy, ceramic, and graphite properties. It exhibits exceptional resistance to high temperature, corrosion, and wear, as well as low density, biocompatibility, and impermeability to liquids and gases. Based on these properties and the low diffusivity of some radioactive elements [7,8] in glassy carbon, glassy carbon is a promising candidate material that can be used as a storage container for nuclear waste.

Glassy carbon must fulfil certain requirements to be applied as a nuclear waste containment material [3,9]. These conditions are: it must be highly resistant to radiation damage from nuclear waste and a good diffusion barrier against radioactive fission elements found in nuclear waste [3,9]. Likewise, the near-surface region structure of the glassy carbon must not change under extreme radiation conditions [3,9]. The applicability of glassy carbon as a diffusion barrier against some radioactive fission products (Cs, Sr, Cd, In, Ag, Se, Xe) have been studied [7,8,17,9–16]. These studies have shown that implantation of fission products into glassy carbon causes some structural changes in the host material (for example, implantation at RT amorphized the glassy carbon while implantation at higher temperature showed less defects in the structure of glassy carbon). However, annealing of the implanted samples resulted in recrystallization of amorphous glassy carbon [7-11,13]. Moreover, the annealing caused the migration of the impurities implanted into the glassy carbon. These studies concluded that the glassy carbon structure played a role in the migration of fission products.

An extensive literature search showed that ruthenium (Ru) in glassy carbon has not been studied previously.$^{106}$Ru (half-life of 373.59 days) is the most stable isotope of rutheniumand it is an important fission product of nuclear fuel or reprocessed nuclear fuel [18]. It can also be obtained by the nuclear transmutation of Technetium-99 ($^{99}$Tc) [19]. Ruthenium fission product is very toxic, and it causes cancer. The purpose of this study is, therefore, to investigate the migration behaviour of implanted Ru in glassy carbon. As was mentioned above, this information is necessary to determine the effectiveness of glassy carbon as a good construction material for the casks used for nuclear waste storage. The structural changes and surface modification due to Ru implantation and annealing were investigated by Raman spectroscopy, X-ray diffractometerand atomic force microscopy.

## 2. Experimental

The glassy carbon (Sigradur®G) samples from Hochtemperatur-Werkstoffe GmbH, Germany, were used in this study. The pristine glassy carbon samples were implanted with 150 keV Ruthenium ions at room temperature (RT) to a fluence of $1\times10^{16}$cm$^{-2}$. The

implantations were done at the iThemba Lab, South Africa. The simulation of the ruthenium implantations into glassy carbon was performed using SRIM 2010 [20]. Fig 1 shows the simulated Ruthenium results: the ruthenium depth profile in glassy carbonalongside the displacements per atom (dpa) caused by the ruthenium ions implantation. The density and displacement energy of glassy carbon were taken to be 1.42 g/cm$^3$ and 20eV in the simulation, respectively. A dpa of 0.2 is required to amorphized glassy carbon [21]. This would imply that the simulation of Ruthenium in the glassy carbon (at the ion fluence of$1\times10^{16}$cm$^{-2}$) resulted in an amorphization thickness of about 155 nm in the glassy carbon substrate. In nuclear waste containers (where glassy carbon can be used), glassy carbon will be exposed to different fission products with different fluences. The defects due to radiation of some of these fission products accumulate in the glassy carbon and may exceed the dpa limit required to amorphize the glassy carbon. Therefore, the structural evolution of glassy carbon under such conditions needs to be investigated.

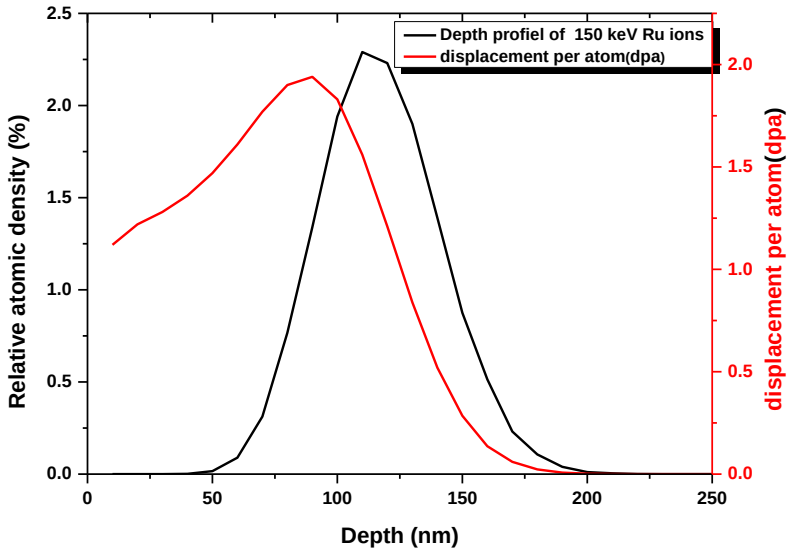


***Fig. 1:*** *Simulated depth profiles of 150 keV ruthenium and displacement per atom (dpa) caused by implantations of ruthenium ions obtained using SRIM 2010 [20].*

The glassy carbon samples implanted with Ru were annealed under vacuum using a computer-controlled *Webb 77* graphite furnace. The samples were isochronally annealed at temperatures ranging from 1000 to 1300 °C in steps of 100 °C for 5 hours.

Atomicforce microscopy (AFM) was used to study the topography of the virgin glassy carbon surfaces after implantation and annealing. The surface topographies were analyzed by a Dimension Icon AFM system in contact mode. The AFM images were recorded at two scales of 20×20 $\mu m^2$. The root mean square (rms) roughness data were obtained by analysing the AFM images using the NanoScope Analysis offline software [22].

Grazing incidence X-ray diffraction (GIXRD) analysis was used to monitor the structural changes of glassy carbon (i.e., phases formation, crystals orientations and sizes, stress and strain in the crystal lattice) after the ruthenium implantation and annealing using the Inorganic Crystalline Structure Database (ICSD) database [23]. GIXRD spectrum of the glassy carbon samples were obtained using a Bruker D8 Discover XRD system with a Cu Kα radiation source (1.54184 Å) at 2θ step size of 0.04°. The incident angle was 4°, and the maximum depth of X-ray in glassy carbon was calculated from the incident angle using the following equation $\tau = 0.5\ L \times sin(\Omega)$ [24], where $\tau$ is the penetration depth, $L$ is path length of X-ray in the sample and Ω is the incident angle. The penetration depth of X-ray in glassy carbon was calculated to be 3 μm.

WITec alpha 300 confocal Raman spectroscopy instrument was used to monitor the effect of ruthenium implantation and annealing on the microstructure of the glassy carbon substrate. A 100×0.9NA objective lens was used to acquire the Raman spectra at the wavelength of 532 nm and laser excitation power of 5 mW. The penetration depth of the 532 nm laser in glassy carbon was calculated using the following equation $z = \lambda / 4\pi k$ [25], and was calculated to be around 59 nm. To analyse the obtained Raman spectra of glassy carbon, the baseline of the spectral lines was corrected using a linear background correction. The Raman spectra of glassy carbon were fitted using both the Gaussian function and the Breit-Wigner-Fano (BWF) functionto determine the width (i.e., full width at half maximum (FWHM)) of the peaks using the OriginLab software program.

The migration behaviour and the depth profiles of the ruthenium in glassy carbon samples before and after annealing was monitored by secondary ion mass spectrometry (SIMS).SIMS analyses were performed with a Cameca IMS 7f microanalyser. For each measurement, a primary beam of 10 keV $O^{2+}$ ions was raster scanned across the sample

area of 150 × 150 $\mu m^2$. The intensity-concentration calibration was achieved with the as-implanted samples as reference. Finally, the depth conversion of the recorded profiles was performed by measuring the sputtered crater depth with a DEKTAK 8 stylus profilometer and assuming a constant erosion rate with time.

## 3. Results and discussion

### 3.1 Raman results

Raman spectra of pristine glassy carbon sample, as-implanted, and annealed sample from 1000 to 1300 °C are shown in Fig. 2. The Raman spectrum of virgin glassy carbon sampleshows the D and G characteristic bands at positions 1346 $cm^{-1}$ and 1587 $cm^{-1}$, respectively. The D and G peaks originate from the disordered $sp^3$ bonds and $sp^2$ vibrations of graphite, respectively [26]. These two peaks of the glassy carbon indicate the presence of small graphitic crystallites (ribbons) imbedded in the amorphous matrix [8]. The D and G peaks merged into a single broadband after implantation, accompanied by a decrease in the peak intensities, indicating amorphization of the graphitic crystallites in the glassy carbon sample [8,26]. The SRIM simulation data presented in Fig. 1, correlates with the Raman data. The amorphization of glassy carbon due to implantation at room temperature, at low implantation energy and at fluences of similar magnitude was also reported by other researchers [7,16,21,27].

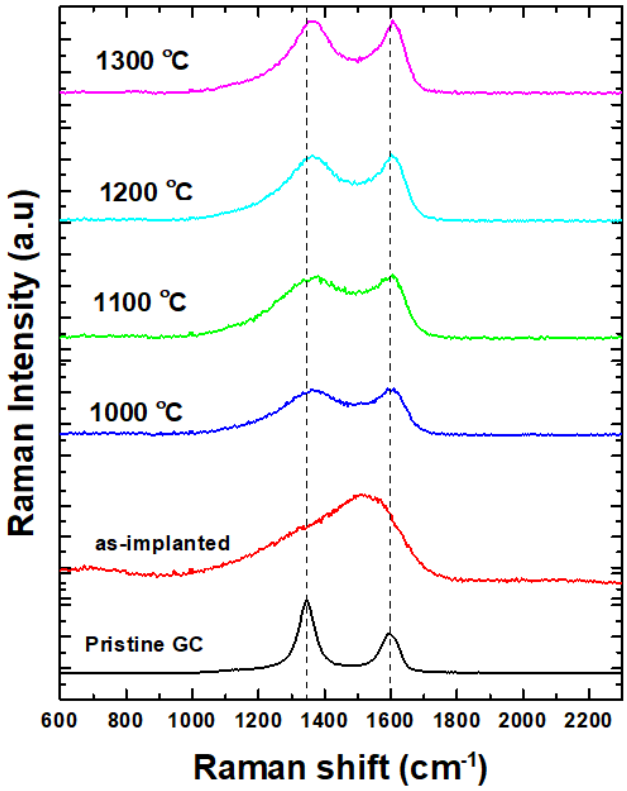


***Fig. 2:*** *Raman spectra of glassy carbon before and after ruthenium implantation at roomtemperature and after annealing the implanted glassy carbon samples from 1000 – 1300°C.*

The initial annealing at 1000 °C showed broad D and G peaks (see Fig. 2), indicating partial recrystallization of glassy carbon after annealing. Further annealing from 1100 °C to 1300 °C resulted in the enhancement of the D and G peaks intensity and a reduction in the peak width. This indicates that some recoveryof the glassy carbon structure increased with the increasing annealing temperature. However, the structure did not return to its original state of the pristine glassy carbon.

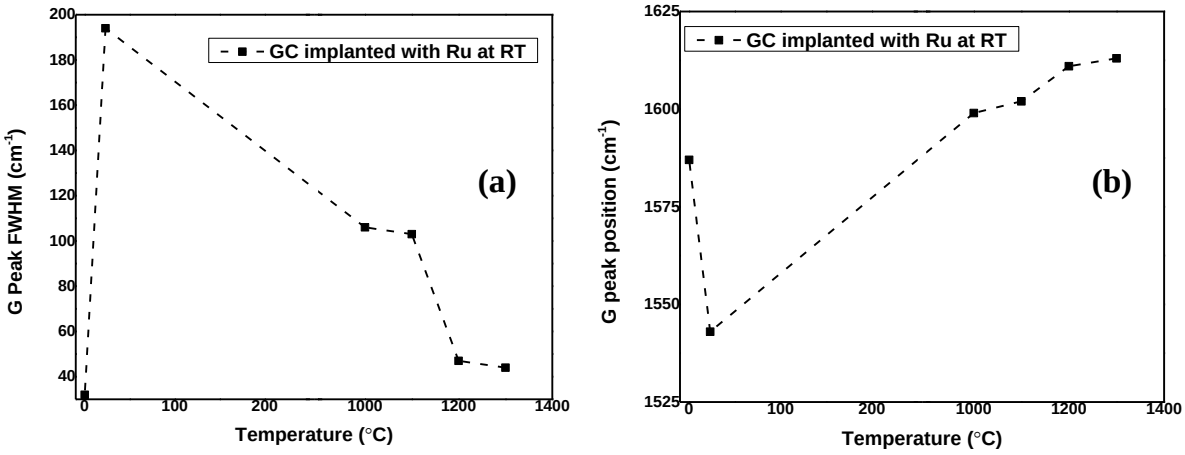


***Fig. 3:*** *The effect of ruthenium ion bombardment at room temperature (i.e., 23 ˚C) and heat treatment on the (a) FWHM values of the G peak of glassy carbon acquired after fitting the spectra with the BWF function and (b) G peak position of the acquired spectra.The G peak position and FWHM of virgin glassy carbon are shown at 0 ˚C.*

Fig. 3 shows the FWHM of the G peaks as well as the positions of the G peaks of the acquired spectra before and after annealing of the glassy carbon samples implanted with Ru. From Fig. 3 (a), the FWHM value of the G peak increased from 31 $cm^{-1}$ (pristine glassy carbon) to 195 $cm^{-1}$ after implantation with Ru at room temperature. This broadening is due to the introduction of disorder (point defects) within the glassy carbon structure [8,13,26,28]. Annealing resulted in the decrease of the FWHM values from 195 $cm^{-1}$ (after implantation) to 42 $cm^{-1}$ (after annealing at 1300 °C). The decrease in the FWHM was an indication of the removal of some defects (annealing of the radiation damage introduced by the ruthenium ion bombardment).

Fig. 3 (b) shows that the G peak position shifts after implantation. This shift of the Raman peak to higher or lower wavenumber can be attributed to stress [29]. The type of residual stress associated with the Raman peak shift to lower wavenumber is tensile stress [29]. Which means the sample was under tensile stress due to the irradiation.

Annealing the as-implanted samples from 1000 to 1300 °C showed a significant shift of the G peak towards thehigher wavenumber which can be attributed to the presence of the compressive stress [29]. These differences in stress between as-implanted and annealed samples could be due to differences in the glassy carbon density after

implantation and annealing [21,30-31]. Several studies by McCulloch *et al.* [21,30-31] found that an increase in the density of virgin glassy carbon after ion implantation at room temperature leads to the introduction of tensile stress in the glassy carbon. McCulloch *et al.* [21,30-31] mentioned that the increase in the density of the implanted glassy carbon will require a smaller volume (since density = mass/volume), then glassy carbon tends to contract, however, is prevented from doing so in the plane of the substrate, giving rise to a tensile biaxial stress.

It is well known that implantation of ions (irrespective of the ions implanted) at room temperature increased the density of virgin glassy carbon [7,21,30-31]. However, Zhang *et al.* [32] found that annealing glassy carbon at temperatures above 1000 °C reduces the density of glassy carbon due to structural rearrangement formation. Reducing the density of the implanted glassy carbon after annealing will result in compressive stress as mentioned by McCulloch *et al.* in ref [30]. McCulloch *et al.* [30] mentioned that the decrease in the density will require a larger volume, thus glassy carbon will tend to expand, however, is prevented from doing so in the plane of the substrate, giving rise to a compressive biaxial stress. This agrees with the result presented in this study, where compressive stress was observed after annealing the as-implanted samples – see Fig.3 (b).

### 3.2 GIXRD

Fig. 4 shows the GIXRD diffractograms for the virgin, as-implanted and annealed glassy carbon. For the virgin glassy carbon (Fig. 4 (a)), the GIXRD reflections at $2\theta = 25.3°$ and 43.4° correspond to a turbostratic carbon structure [33-34]. The reflections at $2\theta = 53.92°$ and 80.5°correspond to hexagonal and orthorhombic graphite, respectively. The GIXRD result, therefore, indicates that the virgin glassy carbon contains amorphous carbon and graphite lattice structures. This result is in good agreement with the Raman result of the virgin glassy carbonin Fig. 2, where the D and G peak of the virgin glassy carbon indicate the presence of small graphitic crystallites imbedded in the amorphous matrix. From Fig. 4 (a), implantation of the glassy carbon with ruthenium ions resulted in a slight peak shift to a lower $2\theta$ position and a decrease in GIXRD peaks intensities accompanied by an increase in their FWHM. This indicates that

ruthenium ions implantation introduced lattice disorder and strain in the glassy carbon crystal structure [35-36].

Fig. 4 (b), shows the GIXRD diffractograms for the as-implanted and annealed glassy carbon. The as-implanted glassy carbon showed broader lower-intensity XRD peaks, compared to the intensities of the peaks of the annealed samples. As mentioned before, the intensityof the individual diffraction peaks depends on the defects of the crystal structure as well as the internal strain of the sample [37]. The internal strain of the virgin, as-implanted and annealed glassy carbon was estimated from GIXRD patterns and shown in Fig. 5.

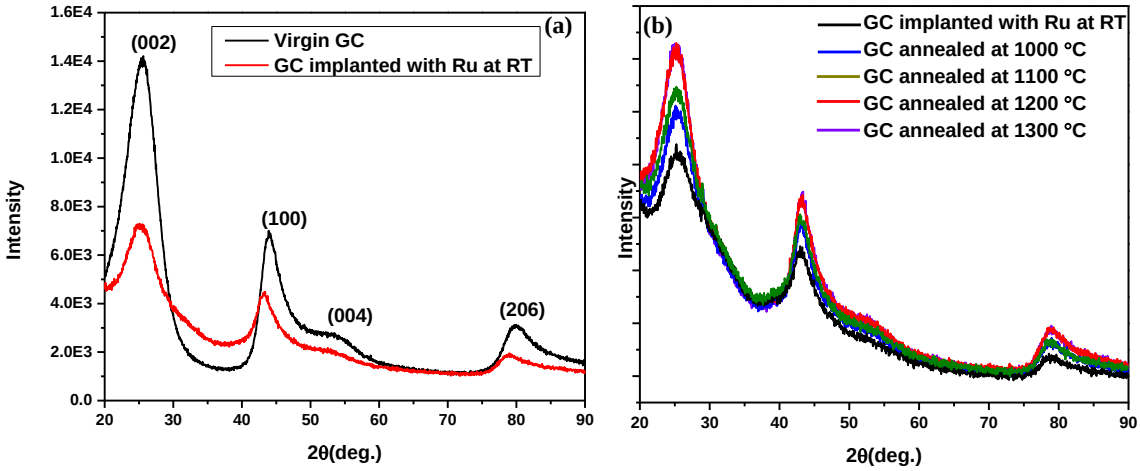


***Fig. 4:*** *The GIXRD diffractograms of (a) virgin and as-implanted glassy carbon (GC), (b) then sequentially annealed at temperatures ranging from 1000 ˚C to 1300 ˚C for 1 h at each temperature..*

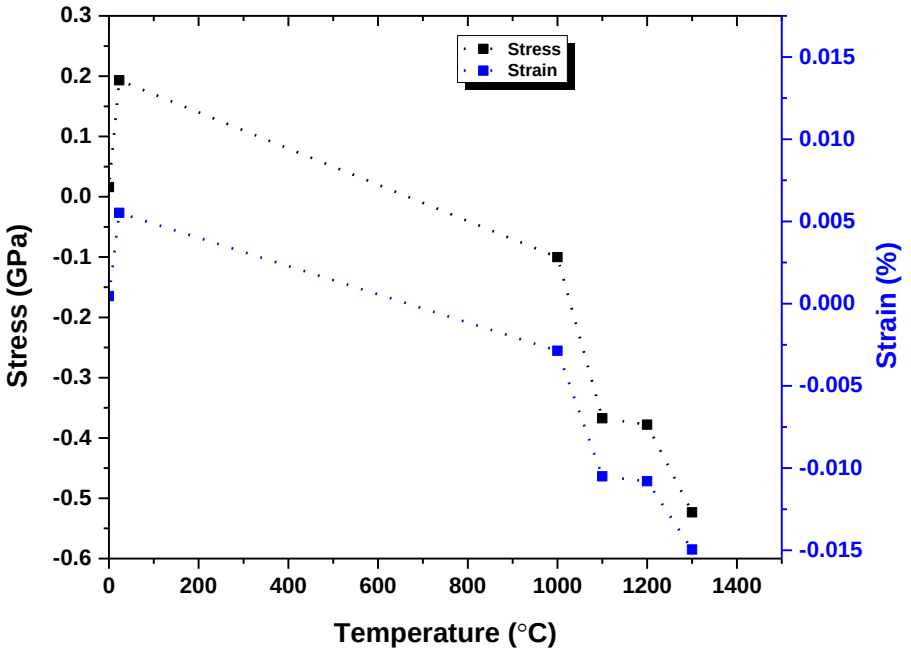


***Fig. 5****: The strain and residual stress of the virgin glassy carbon (at 0 ˚C) after implantation (at room temperature, i.e., 23 ˚C) and annealing obtained from GIXRD.*

Fig. 5 and Table 1show the quantitative stress and strain estimated from GIXRD patterns. The residual strain was obtained by multiplying Young's modulus of glassy carbon (i.e., 35 GPa) by the obtained strain using the Williamson-Hall equation [38]. The amount of stress in virginglassy carbon increased from 0.016 GPa to 0.19 GPa after ion implantation (see Table 1), indicating that ion bombardment caused radiation damage (i.e., disorder within the graphitic crystallites in the glassy carbon structure) [39]. However, the stress of annealed samples has negative values. The minus sign or plus sign in the amount of stress indicates the type of stress: the minus sign indicates compressive stress, while the plus sign indicates tensile stress [40]. Therefore, as seen in Table 1, implantation of ruthenium in glassy carbon produced tensile stress, while annealing the as-implanted samples introduced compressive stress in the glassy carbon. This is in good agreement with Raman's results in the above section, where the G peak position of virgin glassy carbon shifted to a lower wavenumber after implantation, indicating the presence

of the tensile stress. However, the G peak shift to a higher wavenumber after annealing, which indicates the presence of the compressive stress. As mentioned above, the difference in stress between as-implanted and annealed samples could be due to differences in the glassy carbon density after implantation and annealing.Since implantation at room temperature increases the density of virgin glassy carbon [7,21,30-31], the implanted glassy carbon will require a smaller volume, then glassy carbon tends to contract, however, it is prevented from doing so in the substrate plane, giving rise to a tensile biaxial stress [7,21,30-31]. Moreover, annealing reduces the density of the implanted glassy carbon [30]. Reducing the density of the implanted glassy carbon after annealing will require a larger volume, meaning that the glassy carbon will tend to expand, however, is prevented from doing so in the plane of the substrate, giving rise to a compressive biaxial stress [7,21,30-31].

***Table 1:*** *The average residual stress and strain of pristine, implanted, and annealed glassy carbon (GC) samples calculated from GIXRD pattern*

| **Sample** | | **Stress in GPa** | **Strain (%)** |
|---|---|---|---|
| Virgin GC | | 0.016 | $4.5\times10^{-4}$ |
| Implanted GC with Ru at RT | | 0.193 | 0.0055 |
| Implanted GC with Ru at RT after annealing | 1000 °C | -0.100 | -0.0028 |
| | 1100 °C | -0.367 | -0.0105 |
| | 1200 °C | -0.378 | -0.0108 |
| | 1300 °C | -0.523 | -0.0150 |

### 3.3 SIMS result

Fig. 6 shows the ruthenium depth profile of the as-implanted samples at room temperature compared with the ruthenium depth profiles obtained after annealing from 1000 to 1300 °C in the step of 100 °C for 5 hours. Implantation at room temperature resulted in a near Gaussian distribution (see Fig. 6) of the implanted ruthenium with FWHM of 59.2 nm. After annealing, an increase in the maximum of the depth profiles

peaks was observed, accompanied by a decrease in the FWHM. This indicates that the ruthenium atoms aggregate (i.e., high ruthenium concentration) in a smaller region (i.e., narrower FWHM) after annealing as compared to the distribution of ruthenium atoms before annealing. Usually, the aggregation of atoms occurs due to cohesive forces between the atoms themselves, which leads to the formation of clusters or particles [41]. Ruthenium atoms havestrong cohesive forces (6.74 eV/atom) [42]; thus, the ruthenium atoms may easily tend to aggregate into "nanoparticles" in the glassy carbon. Several studies have shown that, during annealing, the metal atoms implanted into the substrate will aggregate to form metal nanoparticles inside the substrate [41,43-46]. In this study, the aggregation of ruthenium atoms after annealing at 1000 °C is accompanied by slight loss (i.e., 6% of total ruthenium atoms) of ruthenium – see Fig. 7. This indicates that some ruthenium atoms diffused through the glassy carbon surface after annealing at this temperature. However, the error in the retained ratio was estimated at 5%. This indicates that the loss of Ru after annealing at 1000 ˚C it can be insignificant because the loss lies within the error bars. The loss of Ru atoms at 1300 ˚C is more significant compared to the loss of Ru atoms at 1000 ˚C – see Fig. 7.

The loss is accompanied by small segregation of ruthenium atoms at the interface between the glassy carbon and the bombardment-induced amorphous region (at a depth of 155 nm below the surface – see Fig. 1).The sizes of Ru and carbon atoms are 130 and 70pm [47] respectively. The significantly larger size of the Ru atom means that a stress field will be created in the surrounding glassy carbon matrix. This stress field will be the cause of the segregation of Ru atoms to the interface where the stress is less.

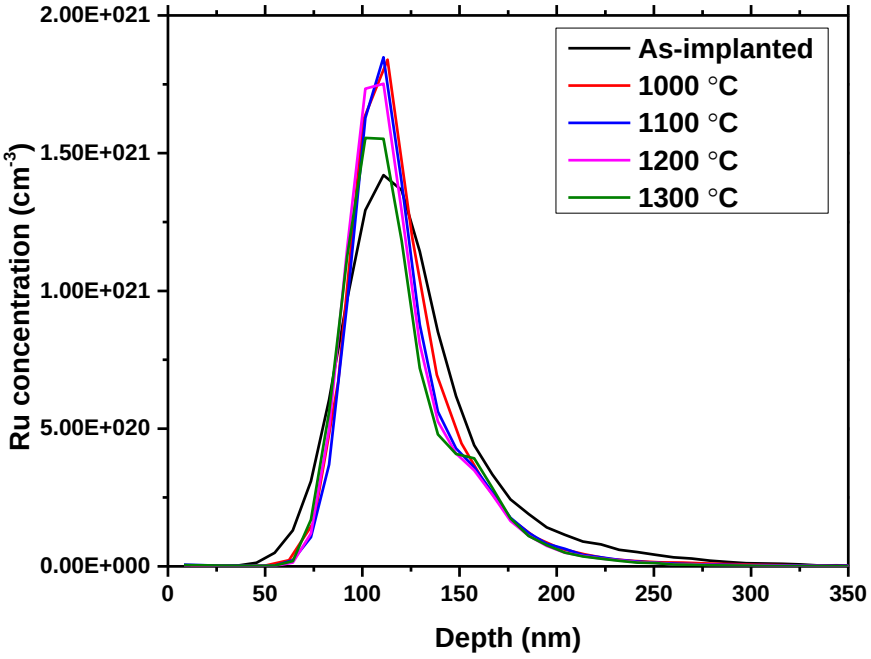


***Fig.6:*** *Depth profiles of ruthenium implanted at room temperature, showing the effect of annealing at high temperature (1000 – 1300°C) on the migration behaviour.*

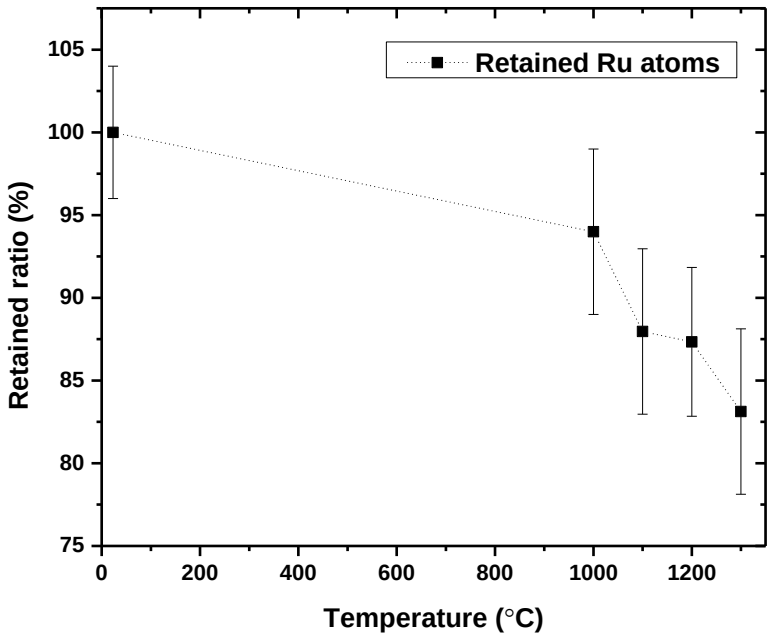


***Fig. 7:*** *Retained ration of ruthenium atoms before and after annealing.*

### 3.4 AFM result

Fig. 8 shows the roughness of the glassy carbon substrate after the Ru ion bombardmentand heat treatment. The surface roughness was evaluated by the AFM images and measured the $R_q$ (root mean square roughness) using the Nanoscope software [22]. The $R_q$ value obtained for virgin glassy carbon is 1.55 nm (see Figs 8 and 9). This value decreased to 0.45 after implantation of ruthenium at room temperature. The reduced surface roughness can be attributed to the ruthenium bombardment. It is widely known that ionbombardment often reduces the surface roughness of an initially rough surface [48] and vice versa (i.e., ion bombardment can increase the surface roughness of an initially smooth surface) [49-51]. In this study, the surface of the initial glassy carbon substrate was rough (i.e., 1.55 nm), and decreased after bombardment by ruthenium ions, indicating that ion bombardment reduced the surface roughness which is consistent with the above statement [48].

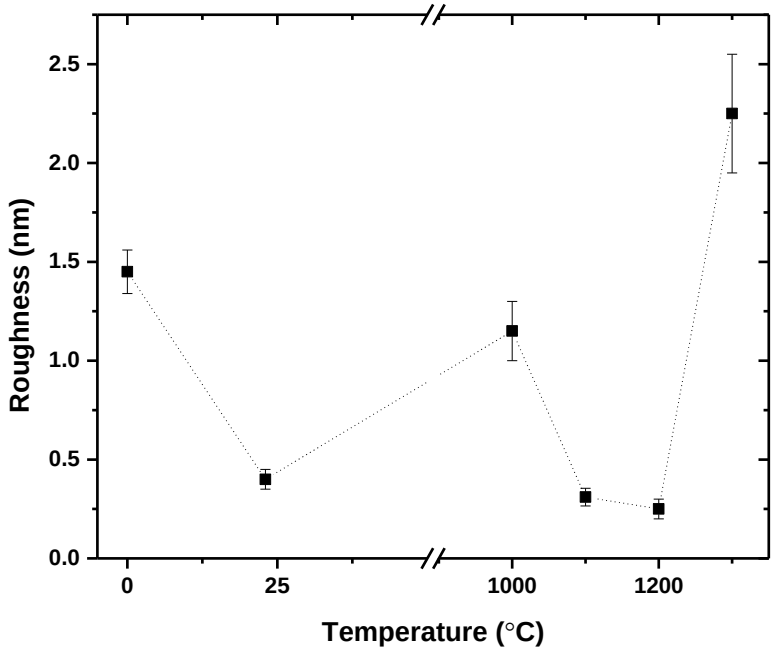


***Fig. 8:*** *Graph showing the effect of ruthenium bombardment at room temperature (i.e., 23 ˚C) and annealing on the surface roughness of virgin glassy carbon (value at at 0 ˚C).*

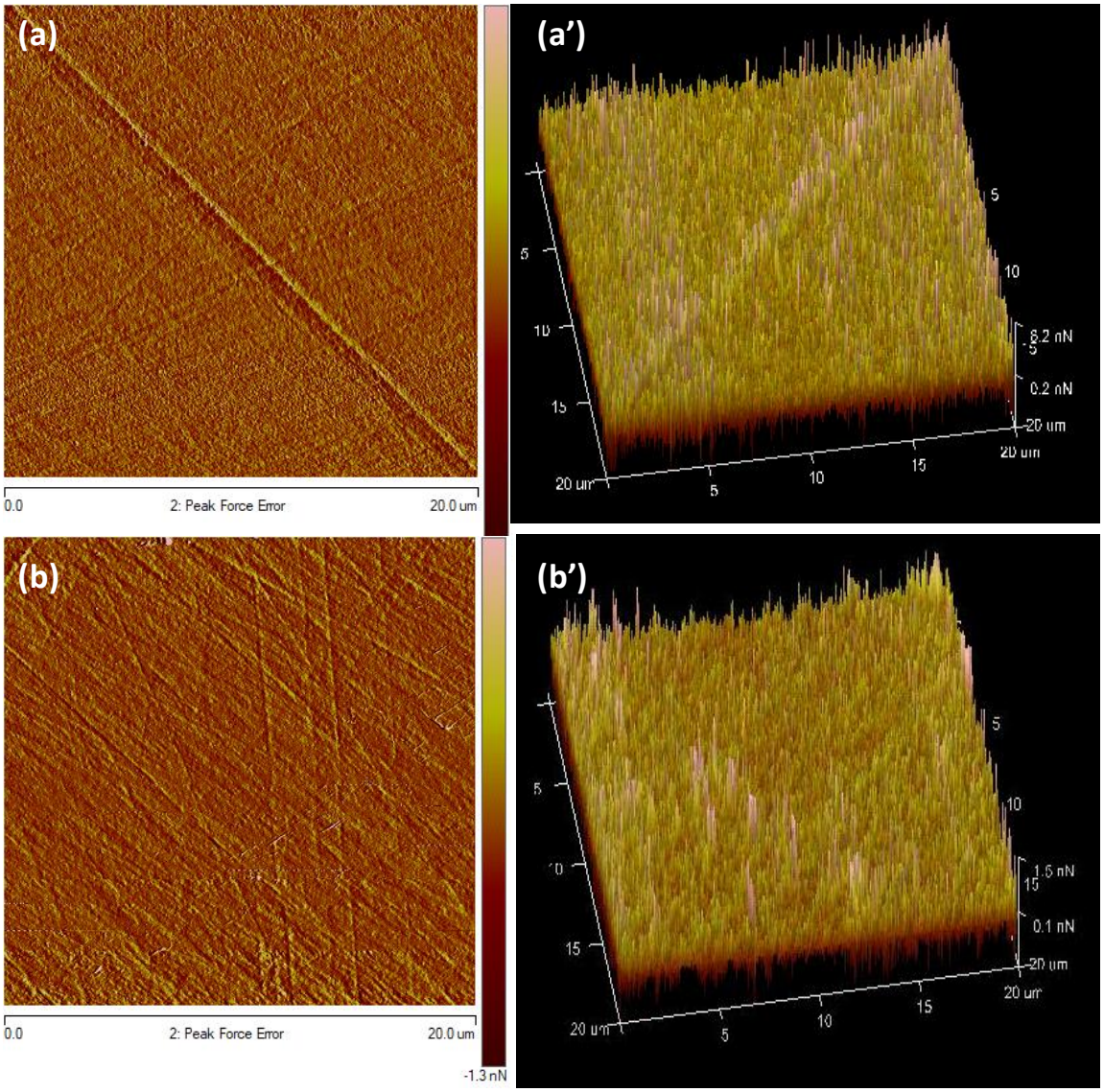


***Fig. 9:*** *AFM images were obtained for (a) virgin glassy carbon and (b) after ruthenium implantation at room temperature. (a') and (b') are the 3D of height images.*

The $R_q$ values obtained from AFM images (in Fig. 10) of annealed glassy carbon samples are shown in Fig.8. As-implanted samples annealed at 1000 °C showed a significant increase in the surface roughness. Aggregation of ruthenium atoms at 1000 °C (see Fig. 6) can lead to the formation of some ruthenium nanoparticles in the near-surface region, thus, increasing the surface roughness of glassy carbon. Naidoo *et al.* [52] found similar results, where the implantation of Ag in amorphous carbon increased the surface roughness due to the formation of Ag nanoparticles in the near surface region. At 1100

and 1200 °C, there was no diffusion/migration of aggregated Ru towards the bulk of the glassy carbon, except for a very slight segregation of Ru atoms (see Fig. 6) at depth of 155 nm. This slight segregation of Ru at these temperatures has no effect on the surface roughness, on the contrary, the annealing reduced the surface roughness (see Fig. 8) due to the surface diffusion of the substrate atoms at the peaks of the sputter roughened surface to valley positions. Clear segregation of Ru atoms was observed (at depth of about 155 nm) after annealing at 1300 ˚C (see Fig. 6). This was accompanied by a loss of Ru– see Fig. 7. Ru atoms were lost through the glassy carbon surface and then probably sublimated into the vacuum of the annealing oven.

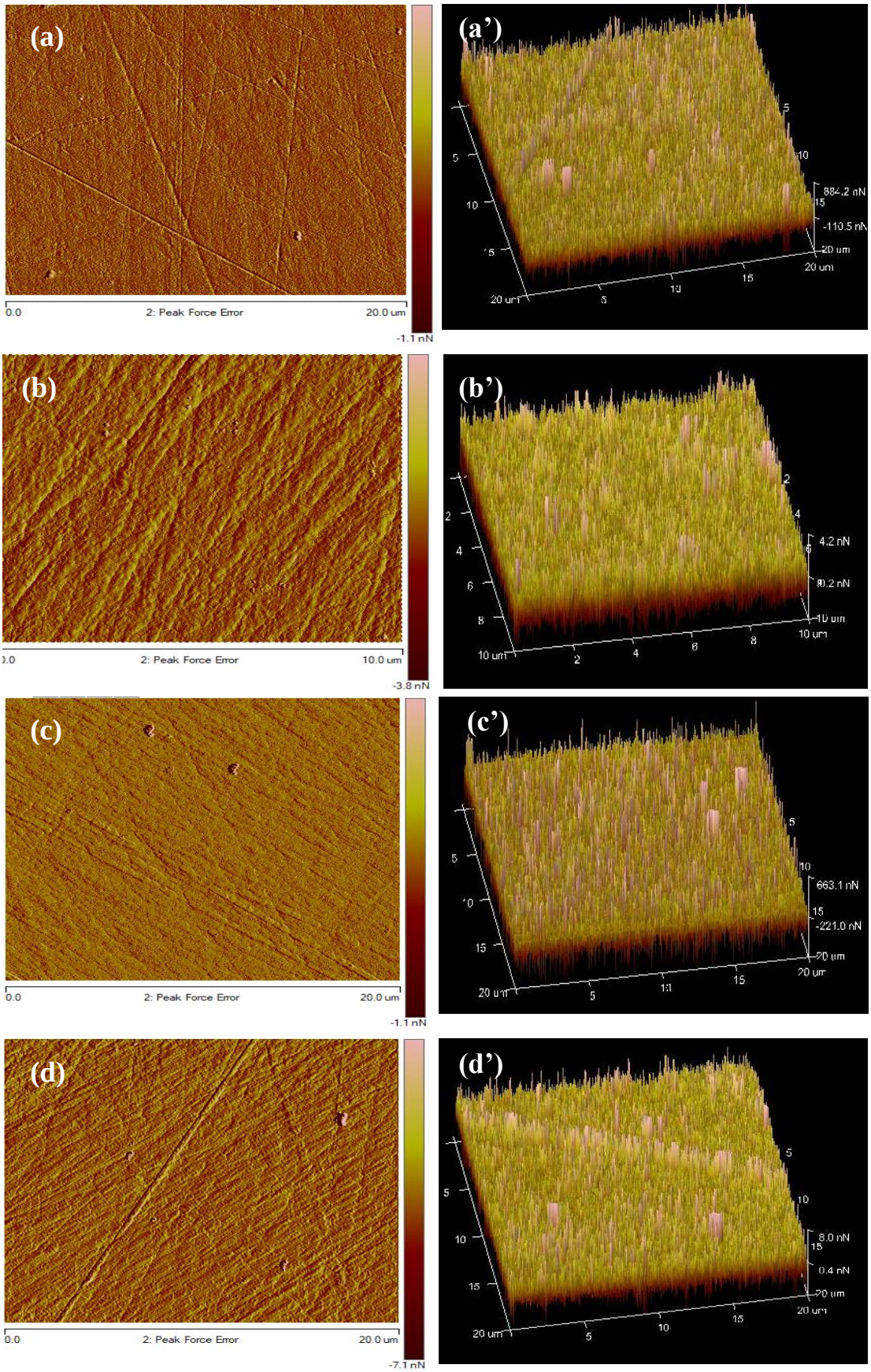
(a)
0.0
2: Peak Force Error
20.0 um
-1.1 nN
(a')
884.2 nN
-110.5 nN
20 um
20 um
(b)
2: Peak Force Error
10.0 um
-3.8 nN
(b')
4.2 nN
10 um
10 um
(c)
0.0
2: Peak Force Error
20.0 um
-1.1 nN
(c')
663.1 nN
-221.0 nN
20 um
20 um
(d)
0.0
2: Peak Force Error
20.0 um
-7.1 nN
(d')
8.0 nN
0.4 nN
20 um
20 um

***Fig. 10:*** *AFM images were obtained for the RT implanted samples annealed at (a) 1000 °C, (b) 1100 °C, (c) 1200 °C and (d) 1300 °C. (a'), (b'), (c') and (d') are the 3D of height images.*

## 4. Conclusion

The effect of ruthenium ions bombardment and annealing on the microstructure of glassy carbon has been investigated using GIXRD, Raman spectroscopy and AFM. Glassy carbonsamples were implanted with 150 keV ruthenium ions to a fluence of $1\times10^{16}$ $cm^{-2}$ at room temperature. The as-implanted samples were vacuum annealed from 1000 to 1300 ˚C in steps of 100 ˚C for 5 hours. GIXRD and Raman spectroscopy showed that ruthenium bombardment caused defects in the glassy carbon structures. These defects were reduced by annealing of the as-implanted samples from 1000 to 1300 ˚C.

Moreover, the effect of annealing on the migration behaviour of implanted ruthenium in glassy carbon has been investigated using SIMS. Implantation at room temperature resulted in a near Gaussian distribution of ruthenium atoms in glassy carbon. Annealing at 1000 ˚C showed an increase in the maximum of the depth profile peak accompanied by a decrease in the FWHM, indicating aggregation of ruthenium atoms. However, after further annealing, limited segregation of ruthenium atoms at the interface between the glassy carbon and the bombardment-induced amorphous region was observed. The significantly larger size of the Ru atom means that a stress field will be created in the surrounding glassy carbon matrix. This stress field was the cause of the segregation and eventual aggregation of Ru atoms to the interface where the stress is less.

AFM results showed that ruthenium bombardment reduced the surface roughness of the virgin glassy carbon. Annealing at 1000 ˚C increased the surface roughness of the as-implanted sample However, at 1100 and 1200 ℃, the roughness of the glassy carbon surface substrate significantly decreased due to the surface diffusion of the substrate atoms at the peaks of the sputter roughened surface to valley positions resulting in reduced visibility of polishing marks. At 1300 ℃, the roughness was significantly increased.

## Declaration of Competing Interest

The authors declare that they have no known competing financial interests or personal relationships that could have appeared to influence the work reported in this paper.

## Acknowledgements

Financial support by the Organization for Women in Science for the Developing World (OWSD) is gratefully acknowledged.The authors wish to thank Dr T. Ntsoane from NECSA for his assistance with XRD data collection. This work is based upon the research supported by the National Research Foundation (NRF) of South Africa (Grant numbers: 132125 and 120808). Any opinion, findings, conclusions, or recommendations expressed in this work are those of the authors and the NRF do not accept any liability regarding thereto. T. T. Thabethe and H. A. A. Abdelbagi acknowledges the financial support from the NRF.

## References


[1] K. Saidi, A. Omri, Reducing $CO_2$ emissions in OECD countries: Do renewable and nuclear energy matter?, Progress in Nuclear Energy 126 (2020) 103425.

[2] B. Merk, D. Litskevich, K.R. Whittle, M. Bankhead, R.J. Taylor, D. Mathers, On a long term strategy for the success of nuclear power, Energies. 10 (2017) 867.

[3] J.B. Malherbe, O.S. Odutemowo, E.G. Njoroge, D.F. Langa, T.T. Hlatshwayo, C.C. Theron, Ion bombardment of glassy carbon, Vacuum. 149 (2018) 19–22. https://doi.org/10.1016/j.vacuum.2017.11.006.

[4] M. V. Ramana, Technical and social problems of nuclear waste, Wiley Interdisciplinary Reviews: Energy and Environment 7 (2018) 289.

[5] R.M. Carranza, M.A. Rodríguez, Crevice corrosion of nickel-based alloys considered as engineering barriers of geological repositories, npj Materials Degradation. 1 (2017) 1-9.

[6] A.J. Innocent, T.T. Hlatshwayo, E.G. Njoroge, T.P. Ntsoane, M. Madhuku, E.O. Ejeh, M. Mlambo, M.Y.A. Ismail, C.C. Theron, J.B. Malherbe, Evaluation of diffusion parameters and phase formation between tungsten films and glassy carbon, Vacuum. 175 (2020) 109245.

[7] S.A. Adeojo, J.B. Malherbe, E.G. Njoroge, M. Mlambo, O.S. Odutemowo, T.T. Thabethe, Z.A.Y. Abdalla, T.T. Hlatshwayo, Effect of sequential isochronal annealing on the structure and migration behaviour of selenium-ion implanted in glassy carbon, Vacuum. 182 (2020) 109689. https://doi.org/10.1016/j.vacuum.2020.109689.

[8] M.Y.A. Ismail, J.B. Malherbe, O.S. Odutemowo, E.G. Njoroge, T.T. Hlatshwayo, M. Mlambo, E. Wendler, Investigating the effect of heat treatment on the diffusion behaviour of xenon implanted in glassy carbon, Vacuum. 149 (2018) 74–78. https://doi.org/10.1016/j.vacuum.2017.12.021.

[9] T.T. Hlatshwayo, L.D. Sebitla, E.G. Njoroge, M. Mlambo, J.B. Malherbe, Annealing effects on the migration of ion-implanted cadmium in glassy carbon,

Nucl. Instruments Methods Phys. Res. Sect. B Beam Interact. with Mater. Atoms. 395 (2017) 34–38. https://doi.org/10.1016/j.nimb.2017.01.086.

[10] E.G. Njoroge, T.T. Hlatshwayo, M. Mlambo, O. Odutemowo, K.A. Annan, A. Skuratov, M. Ismail, J.B. Malherbe, Effect of thermal annealing on SHI irradiated indium implanted glassy carbon, Nucl. Inst. Methods Phys. Res. B. 502 (2021) 66–72. https://doi.org/10.1016/j.nimb.2021.06.011.

[11] E.G. Njoroge, L.D. Sebitla, C.C. Theron, M. Mlambo, T.T. Hlatshwayo, O.S. Odutemowo, V.A. Skuratov, E. Wendler, J.B. Malherbe, Structural modification of indium implanted glassy carbon by thermal annealing and SHI irradiation, Vacuum. 144 (2017) 63–71. https://doi.org/10.1016/j.vacuum.2017.07.020.

[12] O.S. Odutemowo, M.S. Dhlamini, E. Wendler, D.F. Langa, M.Y.A. Ismail, J.B. Malherbe, Effect of heat treatment on the migration behaviour of Sr and Ag CO-implanted in glassy carbon, Vacuum. 171 (2020) 109027. https://doi.org/10.1016/j.vacuum.2019.109027.

[13] O.S. Odutemowo, J.B. Malherbe, L. Prinsloo, D.F. Langa, E. Wendler, High temperature annealing studies of strontium ion implanted glassy carbon, Nucl. Instruments Methods Phys. Res. Sect. B Beam Interact. with Mater. Atoms. 371 (2016) 332–335. https://doi.org/10.1016/j.nimb.2015.10.054.

[14] D.F. Langa, N.G. Van Der Berg, E. Friedland, J.B. Malherbe, A.J. Botha, P. Chakraborty, E. Wendler, W. Wesch, Heat treatment of glassy carbon implanted with cesium at room and high temperatures, Nucl. Instruments Methods Phys. Res. Sect. B Beam Interact. with Mater. Atoms. 273 (2012) 68–71. https://doi.org/10.1016/j.nimb.2011.07.041.

[15] O.S. Odutemowo, J.B. Malherbe, C.C. Theron, E.G. Njoroge, E. Wendler, In-situ RBS studies of strontium implanted glassy carbon, Vacuum. 126 (2016) 101–105. https://doi.org/10.1016/j.vacuum.2016.01.024.

[16] M.Y.A. Ismail, Z.A.Y. Abdalla, E.G. Njoroge, O.S. Odutemowo, T.T. Hlatshwayo, E. Wendler, V. A. Skuratov, J. B. Malherbe, Effect of high

temperature annealing and SHI irradiation on the migration behaviour of Xe implanted into glassy carbon, Nucl. Inst. Methods Phys. Res. B. 489 (2021) 11–19. https://doi.org/10.1016/j.nimb.2020.12.012.

[17] S. Adeojo, J. Malherbe, A. Azarov, O. Odutemowo, E. Njoroge, H. Abdelbagi, S. Mpelane, T. Hlatshwayo, Effects of implantation temperature and annealing on structural evolution and migration of Se into glassy carbon, Solid State Sci. 129 (2022) 106914. https://doi.org/10.1016/j.solidstatesciences.2022.106914.

[18] O. Masson, G. Steinhauser, D. Zok, O. Saunier, H. Angelov, D. Babić, V. Bečková, J. Bieringer, M. Bruggeman, C.I. Burbidge, S. Conil, A. Dalheimer, L.E. De Geer, A. De Vismes Ott, K. Eleftheriadis, S. Estier, H. Fischer, M.G. Garavaglia, C. Gasco Leonarte, K. Gorzkiewicz, D. Hainz, I. Hoffman, M. Hýža, K. Isajenko, T. Karhunen, J. Kastlander, C. Katzlberger, R. Kierepko, G.J. Knetsch, J. Kövendiné Kónyi, M. Lecomte, J.W. Mietelski, P. Min, B. Møller, S.P. Nielsen, J. Nikolic, L. Nikolovska, I. Penev, B. Petrinec, P.P. Povinec, R. Querfeld, O. Raimondi, D. Ransby, W. Ringer, O. Romanenko, R. Rusconi, P.R.J. Saey, V. Samsonov, B. Šilobritiene, E. Simion, C. Söderström, M. Šoštarić, T. Steinkopff, P. Steinmann, I. Sýkora, L. Tabachnyi, D. Todorovic, E. Tomankiewicz, J. Tschiersch, R. Tsibranski, M. Tzortzis, K. Ungar, A. Vidic, A. Weller, H. Wershofen, P. Zagyvai, T. Zalewska, D. Zapata García, B. Zorko, Airborne concentrations and chemical considerations of radioactive ruthenium from an undeclared major nuclear release in 2017, Proc. Natl. Acad. Sci. U. S. A. 116 (2019) 16750–16759. https://doi.org/10.1073/pnas.1907571116.

[19] R.J.M. Konings, R. Conrad, Transmutation of technetium - results of the EFTTRA-T2 experiment, J. Nucl. Mater. 274 (1999) 336–340. https://doi.org/10.1016/S0022-3115(99)00107-5.

[20] J. F. Ziegler, M. D. Ziegler, J. P. Biersack, SRIM – The stopping and range of ions in matter (2010), Nucl. Instrum. Methods Phys. Res. B 268 (2010) 1818–1823.

[21] D. McCulloch, S. Prawer, A. Hoffman, Structural investigations of xenon-ion beam-irradiated glassy carbon, Phys. Rev. B 50 (1994) 5905-5917.

[22] NanoScope Command Reference Manual (2004) Digital Instruments, Version 6.13.

[23] G. Bergerhoff, R. Hundt, R. Sievers, I. D. Brown, The inorganic crystal structure data base, Journal of chemical information and computer sciences. 23 (1983) 66-69.

[24] J. Liu, R.E. Saw, Y.H. Kiang, Calculation of effective penetration depth in X-ray diffraction for pharmaceutical solids, Journal of pharmaceutical sciences. 99 (2010) 3807-3814.

[25] Z. Ni, Y. Wang, T. Yu, Z. Shen, Raman spectroscopy and imaging of graphene, Nano Res. 1 (2008) 273-291.

[26] A. Orlando, F. Franceschini, C. Muscas, S. Pidkova, M. Bartoli, M. Rovere and A. Tagliaferro, A comprehensive review on Raman spectroscopy applications, Chemosensors 9 (2021) 262.

[27] K. Niwase, T. Tanabe, I. Tanaka, Annealing experiment of ion irradiated graphite by laser Raman spectroscopy, J. Nucl. Mater. 191 (1992) 335-339.

[28] K. Niwase, Irradiation-induced amorphization of graphite, Phys. Rev. B 52 (1995) 15785-15798.

[29] E. Wendler, T. Bierschenk, F. Felgenträger, J. Sommerfeld, W. Wesch, D. Alber, G. Bukalis, L. C. Prinsloo, N. van der Berg, E. Friedland, J. B. Malherbe, Damage formation and optical absorption in neutron irradiated SiC, Nucl. Instrum. Methods Phys. Res. Sect. B 286 (2012) 97 – 101.

[30] D. McCulloch, D. R. McKenzie, S. Prawer, Compressive stress induced formation of preferred orientation in glassy carbon following high-dose $C^+$ implantation, Philosophical Magazine A. 72 (1995) 1031-1041.

[31] D. McCulloch, S. Prawer, The effect of annealing and implantation temperature on the structure of C ion-beam-irradiated glassy carbon, Journal of applied physics. 78 (1995) 3040-3047.

[32] Z. L. Zhang, R. Brydson, Z. Aslam, S. Reddy, A. Brown, A. Westwood, B. Rand, Investigating the structure of non-graphitising carbons using electron energy loss spectroscopy in the transmission electron microscope, carbon. 49 (2011) 5049-5063.

[33] S. Manavalan, P. Veerakumar, S. Chen, K. Murugan, K. Lin, Binder-free modification of a glassy carbon electrode by using porous carbon for voltammetric determination of Nitro Isomers, ACS Omega, 4 (2019) 8907−8918.

[34] R. B. More, J. C. Bokros, Biomaterials: carbon, Encyclopedia of medical devices and instrumentation (2006).

[35] A. D. Prasetya, M. Rifai, H. Miyamoto, X-ray diffraction (XRD) profile analysis of pure ECAP-annealing Nickel samples, Journal of Physics: Conference Series 2020 (Vol. 1436, p. 012113).

[36] J. F. Jue and A. V. Virkar, Fabrication, Microstructural Characterization, and Mechanical Properties of Polycrystalline t', Zirconia, J. Am. Ceram. SOC. 73 (1990) 3650-3657.

[37] A. A. Ramadan, A. A. Abd El-Mongy, A. M. El-Shabiny, A. T. Mater, S. H. Mostafa, E. A. El-Sheheedy, H. M. Hashem, Addressing difficulties in using XRD intensity for structural study of thin films, Crystal Research and Technology: Journal of Experimental and Industrial Crystallography 44 (2009): 111-116.

[38] G. K. Williamson, W. H. Hall, X-ray line broadening from filed aluminium and wolfram, Acta metallurgica. 1(1953) 22-31.

[39] R. A. Khmelnitsky, V. A. Dravin, A. A.Tal, M. I. Latushko, A. A. Khomich, A. V. Khomich, A. S. Trushina, A. A. Alekseev, S. A. Terentiev, Mechanical stresses and amorphization of ion-implanted diamond, Nucl. Instrum. Meth. Phys. Res. B 304 (2013) 5-10.

[40] XG. C. Janssen, Stress and strain in polycrystalline thin films, Thin solid films. 515 (2007) 6654-6664.

[41] J. E. Lennard-Jones, The migration and aggregation of atoms on solid surfaces, Proceedings of the Physical Society (1926-1948), 1937 Aug 31, 49(4S) 140.

[42] E. Kaxiras. Atomic and Electronic Structure of Solids. Cambridge: Cambridge University Press, 2003.

[43] G. W. Arnold, J. A. Borders, Aggregation and migration of ion-implanted silver in lithia-alumina-silica Glass. J. Appl. Phys. 48 (1977) 1488–1496.

[44] R. A. Wood, P. D. Townsend, N. D. Skelland, D. E. Hole, J. Barton, C. N. Afonso, Annealing of ion implanted silver colloids in glass. J. Appl. Phys. 74 (1993) 5754–5756.

[45] A. Miotello, G. D. Marchi, G. Mattei, P. Mazzoldi, C. Sada, Clustering of gold atoms in ion-implanted silica after thermal annealing in different atmospheres. Phys. Rev. B 63 (2001) 075409.

[46] V. Resta, G. Quarta, L. Maruccio, L. Calcagnile, Copper ion implantation of polycarbonate matrices: Morphological and structural properties, Nucl. Instrum. Meth. Phys. Res. B 331 (2014) 187-190.

[47] J.C. Slater, Atomic radii in crystals, The Journal of Chemical Physics. 41 (1964) 3199-3204.

[48] M.A. Makeev, R. Cuerno, A. Barabasi, Morphology of ion-sputtered surfaces, Nucl. Instr. and Meth. in Phys. Res. B 197 (2002) 185–227.

[49] Y. Y. Chang, Y. N. Shieh, H. Y. Kao, Optical properties of TiO2 thin films after Ag ion implantation, Thin Solid Films 519 (2011) 6935-6939.

[50] O.S. Odutemowo, J.B. Malherbe, L.C. Prinsloo, EG Njoroge, R. Erasmus, E. Wendler, A. Undisz, M. Rettenmayr, Structural and surface changes in glassy carbon due to strontium implantation and heat treatment, J. of Nucl. Materials 498 (2018) 103-116.

[51] A. Barabasi, H.E. Stanley, Fractal Concepts in Surface Growth, Cambridge University Press, Cambridge, 1995.

[52] S.R. Naidoo, A. Ismaila, Fluence enhanced optical response of Ag implanted amorphous carbon thin films, C. 5 (2019) 45.